Article

Journal of the Brazilian Chemical Society

https://dx.doi.org/10.21577/0103-5053.20240067

J. Braz. Chem. Soc. **2024**, *35*, 9, e-20240067, 1-10

Active Ni-Titanate Nanostructures for Dry Reforming of Methane

Wesley F. Monteiro,[a] Vinícius Demétrio da Silva,[a] Michele O. Vieira,[a] Camila O. Calgaro,[b,c] Oscar W. Perez-Lopez,[b] Marcus Seferin[a] and Rosane A. Ligabue[a,]*

[a]*Programa de Pós-Graduação em Engenharia e Tecnologia de Materiais, Pontifícia Universidade Católica do Rio Grande do Sul (PUCRS), 90619-900 Porto Alegre-RS, Brazil*

[b]*Programa de Pós-Graduação em Engenharia Química, Escola de Engenharia, Universidade Federal do Rio Grande do Sul (UFRGS), 90040-060 Porto Alegre-RS, Brazil*

[c]*Departamento de Engenharia Química, Instituto Federal Sul-Rio-Grandense (IFSul), Campus Pelotas, 96015-360 Pelotas-RS, Brazil*

One of the main causes of climate change is the increased concentration of greenhouse gases from anthropogenic sources. Therefore, the search for processes that provide mitigation of these gases is imperative and very important. Dry reforming of methane (DRM) is a process that converts CO_2 and CH_4 in pure syngas. Thus, this study aims to evaluate the influence of the calcination temperature (500 and 700 °C) in the titanate nanotubes (TNT) structure. The calcination at 700 °C led to a new morphology in the form of titanate nanorods (TNR). TNT and TNR nanostructures were modified with Ni and used as catalysts in the DRM reaction. The CO_2 and CH_4 conversions were around 60 and 48%, respectively, when using Ni-TNT500 at 700 ºC, while values around 85 and 70%, respectively, were obtained using TNR in the same reactional condition. Both catalysts presented values of H_2/CO ratio near 1.

Keywords: titanate nanotube, titanate nanorods, nickel, DRM, syngas synthesis

Introduction

Global warming is a concerning and challenging issue since it is the main cause of climate change due to the increased concentration of greenhouse gases (GHG) from anthropogenic sources.[1-3] In 2015, the Paris Agreement established as a long-term goal, the GHG emissions reduction in order to limit the increase in temperature to 1.5 °C above pre-industrial levels, recognizing that this would significantly reduce the risks and impacts of climate change.[4,5] Carbon dioxide (CO_2) is the main gas emitted in the burning of fossil fuels, especially in the conventional energy industry, which makes it the main greenhouse gas. In addition, CO_2 is a thermodynamically stable molecule needing harsh conditions for chemical transformations to occur.[6-9] On the other hand, methane (CH_4) is the main product derived from the uncontrolled degradation of biomass.[10] In open dumps and landfills, the chemical composition of the landfill gas generated by the decomposition of solid urban waste is basically CH_4 (60%) and CO_2 (40%).[11] Current data from 2023 of the National Oceanic Atmospheric Administration (NOAA) show the atmospheric concentration of CH_4 (1.92 ppm) and CO_2 (423.28 ppm).[12] Despite the low CH_4 concentration relative to that of CO_2, its global warming potential (GWP) is around 30 times higher, contributing considerably to the climate imbalance.[13-15] Hence, carbon capture and storage (CCS) technologies of greenhouse gases are considered fundamental strategies to mitigate environmental impacts.[16-19] Once captured and stored, these gases can be used as precursors in the production of chemicals and power through steam reforming of methane (SRM) (equation 1), partial oxidation of methane (POM) (equation 2) and dry reforming of methane (DRM) (equation 3), where ΔH_{298K} is the enthalpy at 298 K.[20-22]

$$CH_4 + H_2O \leftrightarrow CO + 3\ H_2 \quad (\Delta H_{298K} = +228\ kJ\ mol^{-1}) \quad (1)$$

$$CH_4 + ½\ O_2 \leftrightarrow CO + 2\ H_2 \quad (\Delta H_{298K} = -22.6\ kJ\ mol^{-1}) \quad (2)$$

$$CH_4 + CO_2 \leftrightarrow 2\ CO + 2\ H_2 \quad (\Delta H_{298K} = +247\ kJ\ mol^{-1}) \quad (3)$$

SRM is an endothermic reaction and needs to be

*e-mail: *e-mail: rligabue@pucrs.br
Editor handled this article: Izaura C. N. Diógenes

operated at high temperatures and with high energy consumption. Catalyst sintering and carbon deposition may hinder the SRM reaction.[23] In POM, the thermal stability control might be difficult. DRM is the most important process in the study of molecules with a single carbon atom (C1 chemistry), which has been getting great attention in recent years,[24,25] due to the fact that converts two types of potential carbon resources (CO_2 and CH_4, greenhouse gases) into useful syngas.[25] Besides that, the DRM reaction produces pure syngas (equation 3, equimolar ratio of CO and H_2) which is appropriate for subsequent Fischer-Tropsch process[26] enabling circular economic chemistry.

However, the DRM process has an important limitation, which is the use of stable catalysts under the reaction conditions (i.e., higher temperature).[27] The catalysts commonly used for DRM include high-cost transition metal (Ru) and low-cost (Ni, Co, Fe) catalysts. The transition metal carbides have also been shown to be active in the transformation of methane into syngas.[28,29] Materials like MgO-ZrO_2, TiO_2-ZrO_2, Nb_2O_5-ZrO_2, TiO_3-Al_2O_3 have been used as supports, with properties to reduce the coke formation on the surface.[30-33]

Noble metal-based catalysts have shown high activity and high resistance to coking (carbon deposition), but they are very expensive and of limited availability. On the other hand, non-noble metal-based catalysts can show similar activity to those based on noble metals, but coke is prone to form, leading to catalyst deactivation.[34] Despite Ni being a noble metal, the nickel-based catalysts present low cost, due to the natural abundance of the metal and good catalytic activity for DRM reaction.[35] In addition to these, when compared to other metals such as Co and Fe, the higher resistance of Ni to oxidation makes it more attractive in the synthesis of highly active catalysts for DRM.[36]

However, they suffer from the main problems related to DRM, which is deactivation by coke accumulation or sintering of the active phase.[37] Among the approaches for improving Ni-based catalysts, the support presents a beneficial effect on the dispersion of active sites due to the metal-support interactions, which prevent rapid catalyst deactivation at high temperatures by accelerating the gasification of deposited carbons.[38,39]

In this context, many catalytic supports have been developed, such as hydrotalcite,[40] perovskite $LaNiO_3$[41] and vanadate nanotubes,[42] among others. In the cases of the coke deposition resistance, interaction metal-support and reducing the sintering active phase were improved. In this context, the search for new supports capable of providing stability for the catalytic system has been a focus in the literature.[43,44]

The material properties optimization through its morphological control has attracted great attention, mainly with regard to the development of similar nanostructures to metal oxides.[45] Titanate nanostructures with low 1D dimension such as nanotubes, nanowires, among others have been applied in areas such as electronics, magneto-electronics, optics, catalysts, sensors, and energy conversion.[46-49] These nanostructures present a structure with TiO_6 octahedrons as building blocks, connected by corner- and edge-sharing oxygen atoms forming negatively charged two-dimensional sheets facilitating ion diffusion, leading to the exchange and intercalation, and the increasing of surface area.[50] Furthermore, titanate nanostructures feature both acidic and basic active sites,[51,52] thereby enhancing the catalytic activity of the system when employed as support.

The application of titanate nanotubes (TNT) modified with different metals as a catalyst has been reported in the literature for reactions such as polyethylene terephthalate (PET) depolymerization,[51] Suzuki-Miyaura cross-coupling,[53] biodiesel synthesis,[54] among other. In relation to DRM reaction, the use of TNT as a catalyst for DRM showed CO_2 and CH_4 conversions around 30 and 35%, respectively, with an H_2/CO ratio of 0.5.[55] Moreover, in our preceding study, we evaluated the interaction of various metals (Co, Cu, Zn, and Ni) with TNT as catalysts in the DRM reaction, where Ni proved to be the most active metal.[56]

Besides these findings, as demonstrated in our previous study,[57] the calcination of TNT results in structural and morphological modifications that enhance its catalytic properties when applied to the synthesis of glycerol carbonate.

In this context, motivated by the low number of studies about the application of TNTs as catalysts for the DRM reaction, as well as the influence on the morphology and structure generated by the calcination of these nanostructures, the presented work aims to evaluating the influence of the calcination temperatures 500 and 700 °C in the TNT structure, where the latter generated a new morphology, titanate nanorods (TNR). These nanostructures were modified with Ni and applied in the DRM reaction.

Experimental

Synthesis of catalysts

TNT were synthesized as described in the literature.[57] In a typical procedure, 18.8 mmol of TiO_2 powder (1.5 g, TiO_2, 98.0% anatase phase, JB Química, Porto Alegre, Brazil) were added to 120 mL of 10 mol L^{-1} NaOH solution (99.0%, Vetec, Duque de Caxias, Brazil) and maintained under magnetic stirring for 30 min. The suspension was

hydrothermally treated in a 100 mL Teflon-lined autoclave at 130 °C for 72 h. After, the white precipitate obtained was washed with distilled water (until the pH of the wash water reached 7), centrifuged and dried at 80 °C for 6 h. The TNT were calcined in two different temperatures (500 and 700 °C). In a typical procedure, 1 g (3.3 mmol) of pristine TNT was calcined in determined temperature (500 or 700 °C) in a muffle with a heating rate of 10 °C min^{-1} for 4 h. This procedure generated titanate nanotubes when calcined at 500 °C (named as TNT500) and TNR when calcined at 700 °C (Scheme 1).

The modified TNT500 and TNR with Ni were obtained by the impregnation method. In a typical procedure, 1 g TNT500 (or TNR) was added to 50 mL of 0.086 mol L^{-1} nickel nitrate solution ($Ni(NO_3)_2{\cdot}6H_2O$, 97.0%, Vetec, Duque de Caxias, Brazil) and kept under magnetic stirring at room temperature for 24 h. Lastly, the solid product was filtered and dried at 80 °C for 12 h. The catalysts were calcined with a heating rate of 10 °C min^{-1}, at 500 °C for 4 h. The samples were named as Ni-TNT500 and Ni-TNR, respectively.

Dry reforming of methane tests

For the DRM reactions, the methodology described in a previous work by our group[56] was followed. For the reaction, it was used a fixed-bed quartz reactor (0.5 inch diameter) heated in an electric oven. Before the reactions, catalysts were activated *in situ* at 700 °C for 1 h, under a mixture of H_2 and N_2 (100 mL min^{-1}, volume ratio H_2:N_2 of 1:9, 10 °C min^{-1} of heating rate). The catalytic tests were performed at temperatures between 500-700 °C. This range of temperatures was evaluated because DRM is a strongly endothermic reaction, requiring high temperatures to activate the highly stable chemical bonds of both CH_4 and CO_2 molecules.[58] The amount of catalyst used was 100 mg, at GHSV (gas hourly space velocity) of 12000 mL g^{-1} h^{-1} (considering only CH_4 and CO_2). The flow rate used in the tests was 100 mL min^{-1} at a CH_4:CO_2:N_2 volume ratio of 1:1:8. Four gas chromatography analyses of 10 min were taken at each temperature. The results were obtained from the mean of these analyses.

The gaseous products resulting from the reaction were analyzed by on-line gas chromatography (Varian 3600cx), with a packed column (Porapak Q, from Merk, Massachusetts, USA), thermal conductivity detector (TCD) and N_2 as the carrier gas. To quantify the methane and carbon dioxide conversion, as well as, H_2/CO ratio, the following equations were used:

$$CH_4 \text{ conversion } (\%) = \frac{(CH_{4(in)} - CH_{4(out)})}{CH_{4(in)}} \times 100 \quad (4)$$

$$CO_2 \text{ conversion } (\%) = \frac{(CO_{2(in)} - CO_{2(out)})}{CO_{2(in)}} \times 100 \quad (5)$$

$$H_2/CO_2 \text{ ratio} = \frac{H_{2(out)}}{CO_{(out)}} \quad (6)$$

Characterization of catalysts

Morphological analysis of the nanostructured catalysts was evaluated by transmission electron microscopy (TEM, FEI Tecnai G2 T20, Thermo Fisher Scientific, Waltham, Massachusetts, USA). The dispersion of nickel over the catalyst was evaluated by field emission scanning electron microscopy (FESEM, FEI Inspect F50, Thermo Fisher Scientific, Waltham, Massachusetts, USA) in secondary electron beam and dispersive energy spectroscopy (EDS) mode.

The dispersed Ni content was evaluated by inductively coupled plasma optical emission spectrometer (ICP-OES) performed in a PerkinElmer equipment, model Optima 7000 DV (Shelton, Connecticut, USA).

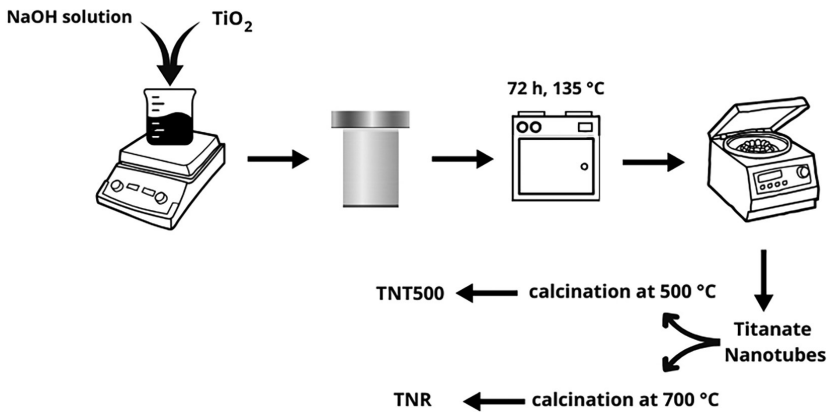

Scheme 1. Illustration of the synthesis procedure of TNT500 and TNR.

Temperature-programmed reduction (TPR) was performed in a multipurpose system (SAMP3), at a heating rate of 10 °C min^{-1} up to 850 °C, total flow rate of 30 mL min^{-1} (volume ratio H_2:N_2 of 1:9).

Thermogravimetric analysis (TGA) and temperature program oxidation (TPO) were performed at a heating rate of 10 °C min^{-1} (from room temperature to 800 °C), under air flow, in an SDT Q600 (TA Instruments, New Castle, USA).

To identify the phases presented in the nanostructures, Raman spectroscopy was performed in a Horiba Scientific-IHR550 spectrometer (Horiba Inc., Kyoto, Japan) using an excitation laser with a wavelength of 531.1 nm.

Results and Discussion

Characterization of catalysts

In order to evaluate the morphology of the nanostructures, TEM analyses were performed (Figure 1). The calcination of the TNT at 500 °C (TNT500, Figure 1a) presented a nanotube morphology formed by at least three walls and with an external diameter of 11.0 ± 2.0 nm, while the calcination of TNT at 700 °C resulted in a change in the morphology, generating a rod morphology (TNR, Figure 1d) with a diameter of 38.3 ± 0.3 nm. These values are higher than reported for TNT, which was 8.8 ± 0.8 nm,[56] and can be attributed to the change in the morphology. The impregnation of Ni on the TNT500 (Figures 1b and 1c) did not affect the tubular morphology and, Ni-TNT500 presented an external diameter of 9.8 ± 0.5 nm. The Ni nanoparticles on the surface of the nanotubes are observed in the TEM analyzes (Figure 1c). In the case of Ni-TNR, it was also observed Ni nanoparticles on the surface of the rods (Figure 1f) and its external diameter reached 60 ± 15 nm, i.e., it occurred an increase in the nanostructure diameter when compared with TNR (38.3 ± 0.3).

Figure 2 shows the EDS mapping of nanostructures. The Ni-TNT500 nanostructure mapping (Figures 2a-2b) indicated the presence of Ni element, in addition to Ti and O. On the other hand, the Ni-TNR mapping (Figures 2c-2d) showed that the TNR is totally covered by Ni, for this reason, it was not possible to identify the Ti and O. These results indicated that Ni was homogeneously dispersed over both nanostructures, and the Ni-TNR nanostructure must have been coated with a higher Ni content.

To determine the concentration of Ni in each sample, ICP analyses were performed. The results for Ni-TNT500 showed that the Ni concentration was 8.95 ± 0.01%, while for Ni-TNR, the value was 2.45 ± 0.21%. Additionally, the concentration of Na in the pristine and Ni-modified nanostructures was determined to verify the possibility of ion exchange between Na and Ni. The result of Na in TNT500 was 8.61 ± 0.07%, and in the Ni-TNT500 was 2.61 ± 0.01%. Regarding the TNR, the value of Na was 4.31 ± 0.05%, and in Ni-TNR was 2.61 ± 0.01%. These results indicate that the calcination at a higher temperature (700 °C) reduces the concentration of Na in the titanate nanostructure when compared to the calcination at 500 °C, and this is correlated with the capacity for Ni modification. Ion exchange is taking place in both nanostructures, but

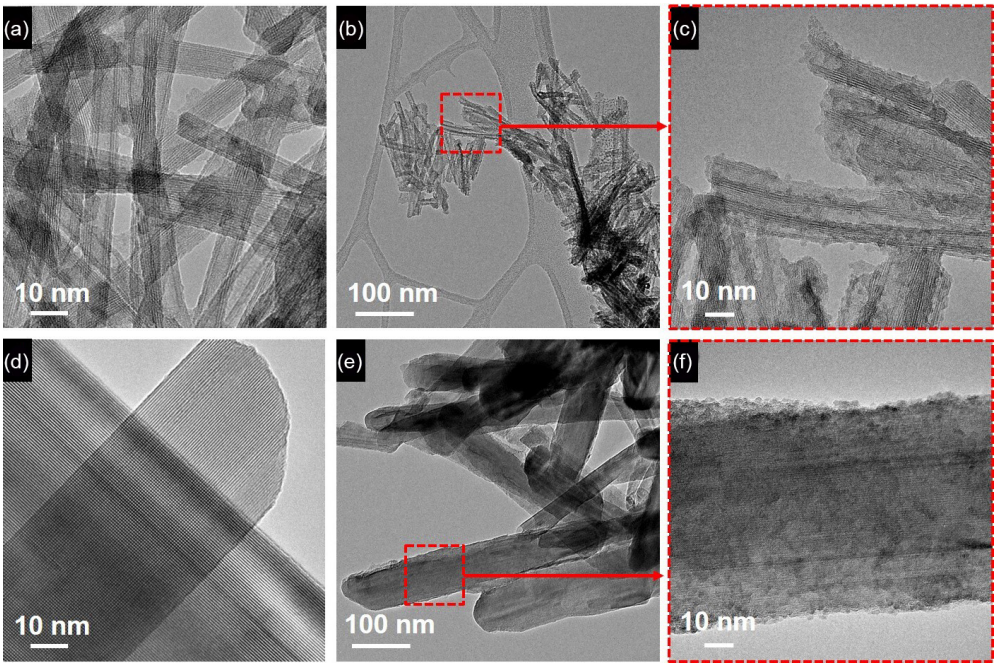

Figure 1. TEM images of (a) TNT500, (b, c) Ni-TNT500, (d) TNR and (e, f) Ni-TNR.

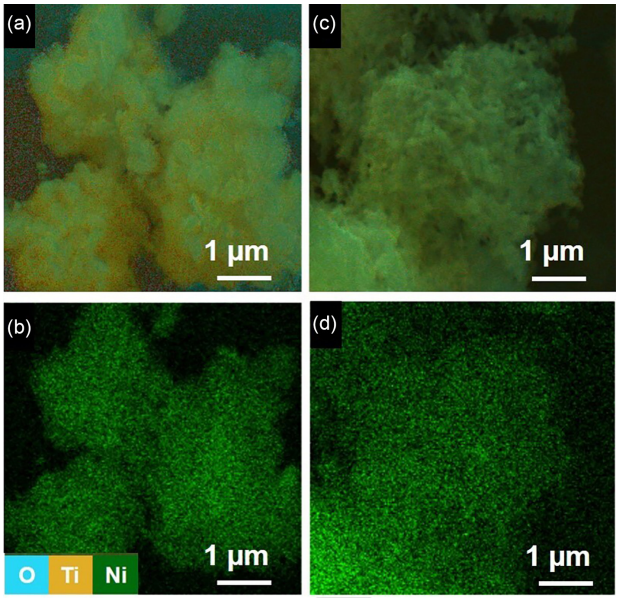

Figure 2. EDS mappings of (a) Ni-TNT500 and (b) and Ni-TNR. Ni mappings of (c) Ni-TNT500 and (d) Ni-TNR.

the effect is more pronounced in TNT500 due to its higher concentration of Na.

The chemical structures of TNT500 and TNR nanostructures were evaluated by Raman analysis (Figure 3a). The TNT500 and TNR spectra present the same characteristic signals of non-calcined titanate nanotubes: 168 and 193 cm^{-1} assigned to Na···O–Ti bending modes and, in 295, 462, 710 and 926 cm^{-1} assigned to Ti–O–Ti stretching from the TiO_6 octahedra from edge-shared TiO_6.[59-61] It was also observed, in the TNR spectrum, bands located at 145 cm^{-1} (anatase phase characteristic), 235 cm^{-1} (rutile phase characteristic) and 900 cm^{-1} assigned to TiO_6.[62]

In order to evaluate the interaction and reduction behavior of incorporated Ni on TNT500 or TNR, TPR analysis was performed (Figure 4). Both samples showed two main peaks, these two peaks corresponding to NiO_x reduction ($NiO \rightarrow Ni°$) to the Ni in the TNT structure.[56,63]

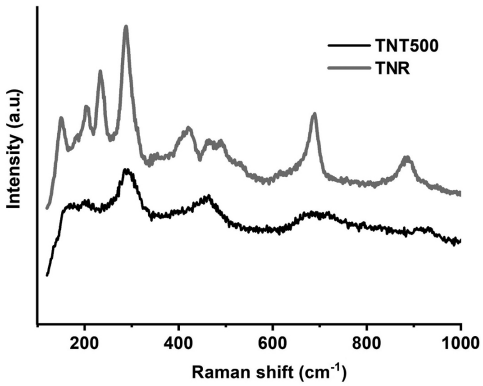

Figure 3. Raman spectra of TNT500 and TNR.

Through deconvolution of the TPR profiles it is possible to identify three reduction peaks as already identified for the Ni-NaTNT catalyst in a previous study.[56] The first deconvoluted peak for Ni-TNT500 was observed at 536 °C, while Ni-TNR showed the first deconvoluted peak at 554 °C. It was possible to observe a displacement of the deconvoluted peaks to higher temperatures comparing Ni-TNT500 and Ni-TNR. In the first, it is observed total reduction at 700 °C, while the second nanostructure presented a part of the material not fully reduced. The reduction peaks at higher temperatures for Ni-TNR indicate a stronger interaction of NiO crystallite with the TNR nanostructure. These results corroborate those obtained by TEM and EDS (Figures 1 and 2), indicating a greater dispersion of Ni on the support. The second and third deconvoluted peaks probably correspond to the reduction of the smallest NiO_x crystallite or NiO_x species with stronger interaction with the support.[56]

Catalytic activity in DRM reactions

Figure 5 shows the study of the reaction temperature in DRM using Ni-TNT500 and Ni-TNR as catalysts. The results are the mean values of four gas chromatography

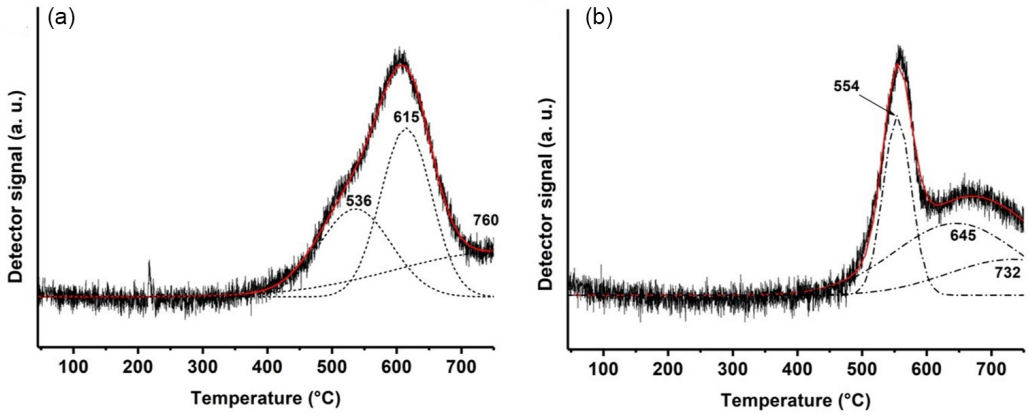

Figure 4. TPR analyses of (a) Ni-TNT500 and (b) Ni-TNR.

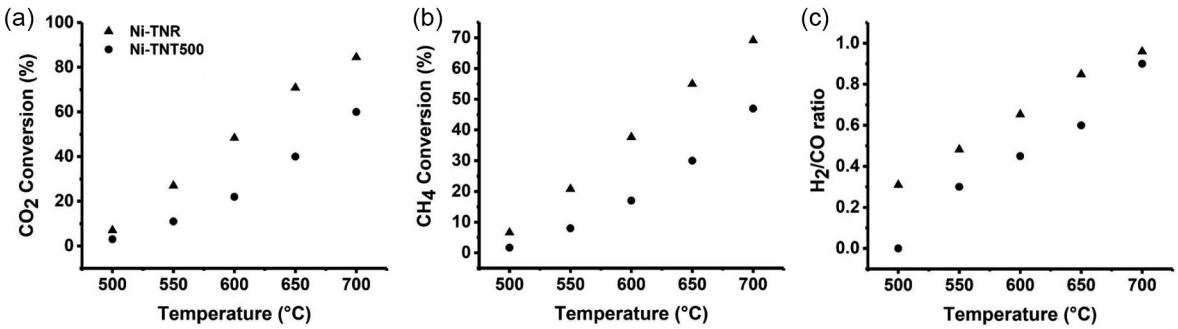

Figure 5. Influence of reaction temperature on (a) CO_2 conversion, (b) CH_4 conversion and (c) H_2/CO ratio in DRM reactions using Ni-TNT500 and Ni-TNR as catalysts.

measurements at each temperature, with a mean standard deviation of 1.20% for CH_4 conversion, 1.81% for CO_2 conversion, and 0.02 for H_2/CO ratio for the reaction with Ni-TNT500. For the reaction with Ni-TNR, the mean standard deviation is 2.29% for CH_4 conversion, 1.94% for CO_2 conversion, and 0.03 for H_2/CO ratio. It was observed that conversions of CO_2 and CH_4 increased as the temperature increased in agreement with the thermodynamics trend (endothermic reaction, equation 3) for both catalysts. For the Ni-TNT500 nanostructure, concerning CO_2 conversion, the values ranged from 7 to 60%, while CH_4 conversion varied from 5 to 48%. To Ni-TNR, the CO_2 conversion increased from 7 to 85% when temperature increased from 500 to 700 °C, while the CH_4 conversion increased from 7 to 70% in the same temperature range. The CO_2 conversions reach equilibrium conversion values from 600 to 700 °C which is about 50 to 80%, respectively. The CH_4 conversions obtained are lower than the thermodynamically predicted equilibrium conversions which can reach around 95% at 700 °C,[64,65] but CH_4 conversions get closer to the equilibrium conversion values as the reaction temperature increases.

Both catalysts showed activity for the DRM reaction, but the Ni-TNR showed higher CO_2 and CH_4 conversions. Comparing the values obtained for the Ni-TNT500 and Ni-TNR nanostructures with the sodium titanate nanotubes modified with Ni (Ni-NaTNT) presented in a previous work,[53] an increase in catalytic activity is observed. Regarding the Ni-TNT500 nanostructure, calcination provided an improvement of approximately 20% in both CO_2 and CH_4 conversion at 700 °C. Evaluating the results of the Ni-TNR nanostructure, it is observed that the morphological modification from nanotubes to nanorods brought significant improvement, with an increase of approximately 50% in both CO_2 and CH_4 conversion. This result is even superior to those obtained with the protonated titanate nanotubes modified with Ni (Ni-HTNT) presented in the previous study,[53] where the best results were 74 and 70% for CO_2 and CH_4 conversion, respectively, at a temperature of 700 °C. The fact that Ni-TNR is the most active indicates the positive effect of the morphology of the rods as support. This activity was probably due to the greater dispersion of Ni on the TNR support, as seen in the TEM and the EDS analysis (Figures 1 and 2). This better Ni dispersion is important in the DRM reaction, in order to avoid the sintering of Ni which normally occurs in this reaction.[66]

It was observed that the H_2/CO ratio also increased with temperature, and it was near to 1 at 700 °C for both catalysts. The H_2/CO ratio close to 1 indicates the favoring of DRM reaction with the increase of temperature, since the DRM reaction is strongly endothermic (equation 3).[65] The H_2/CO ratio near to 1 obtained at 700 °C demonstrates the catalysts selectivity for the DRM reaction, leading to believe that the undesirable reactions which formed carbon and consume hydrogen, such as reverse water gas shift, were minimized. The higher CO_2 conversion compared to CH_4 conversion and the consequent smaller H_2/CO ratio at lower temperatures (from 500 to 650 °C) were due to occurrence of others reactions, mainly of reverse water gas shift ($CO_2 + H_2 \rightarrow CO + H_2O$) which is less endothermic than the DRM reaction.[65]

Table 1 presents the selectivity of H_2 and CO formed using each catalyst. Initially, at 500 °C, both catalysts exhibit higher selectivity for CO. However, as the temperature increases, the selectivity for CO decreases while the selectivity for H_2 increases. Throughout all temperatures, the Ni-TNR catalyst demonstrates superior selectivity for H_2. At 700 °C, the selectivity for H_2 and CO becomes more comparable, as the dry methane reforming reaction is favored at higher temperatures. Nevertheless, it is evident that the methane conversion at 700 °C remains lower than the CO_2 conversion and the equilibrium conversion for the given reagent feed condition (approximately 90%), which affects the selectivity of the products.

As observed, the Ni-TNR catalyst exhibited superiority compared to Ni-TNT500, which may be attributed to improved metal-support interaction, as evidenced in the

Table 1. Selectivity of H_2 and CO formed using each catalyst

Temperature / °C	Ni-TNT500		Ni-TNR	
	H_2 selectivity / %	CO selectivity / %	H_2 selectivity / %	CO selectivity / %
500	–[a]	–[a]	23.62	76.38
550	21.21	78.79	32.52	67.48
600	30.32	69.67	39.51	60.49
650	37.75	62.26	45.90	54.10
700	46.84	53.16	48.95	51.05

[a]Due to the low initial conversion of the reagents, it was difficult to monitor the CO formed.

TPR results (Figure 4). Despite the lower Ni concentration detected in the ICP results for the Ni-TNR catalyst, the metal exhibits a stronger bond with the support, thereby enhancing the stability of the catalytic system and consequently increasing catalytic activity.

In addition to the differences in the interaction of Ni with the support, there are variations in the titanate nanostructures used. Comparing the results of this study with our previous research,[56] which evaluated the use of sodium titanate nanotubes and protonated titanate nanotubes (NaTNT and HTNT, respectively), superior outcomes are observed for the DRM reaction. As the main difference lies in the catalytic supports employed, the observed enhancement in catalytic activity may be associated with the morphological and structural differences of the supports after heat treatment at 500 and 700 °C, as assessed in this study. As evaluated in our previous study,[57] the calcination at 500 and 700 °C induces an increase in the Ti^{2+} concentration at the expense of Ti^{4+} species, along with slight decline in the peaks observed at 458 and 464 eV, corresponding to the binding energy of Ti $2p_{3/2}$ and Ti $2p_{1/2}$, respectively. These distinctions suggest an elevation in electron density and a reduction in the Lewis acidity of the titanium atom, which appears to favor an increase in the catalytic activity of the nanostructures used as supports.

Spent catalyst characterization

After the use of the Ni-TNT500 and Ni-TNR catalysts in the DRM reactions, TEM analyzes were performed (Figure 6) to evaluate the formed coke on the surface of the catalysts. Carbon is mainly formed by the decomposition reaction of methane,[67] which in this study may have been minimized using a feed ratio of $CH_4/CO_2 = 1$. This condition, added to the characteristics of the catalyst, resulted in low carbon formation. Carbon deposition during a DRM reaction can generate three carbon types that are commonly reported in the literature: (*i*) amorphous carbon, (*ii*) graphitic carbon and (*iii*) filamentous carbon.[56,67] In a previous study from our group,[56] a mechanism of carbon deposition was proposed using Ni-TNT as a catalyst. As observed in the current study, using Ni-TNT500 and Ni-TNR, metal nanoparticles are found on the tips and inside of the filamentous carbon, showing that these catalysts favored base-growth mechanisms.[68] For Ni-TNT500, it is observed only encapsulating carbon, and for the Ni-TNR a small amount of filamentous carbon is observed. Carbon deposition could weaken the interaction between metallic Ni and support, resulting in agglomerations.[25]

The carbon amount produced in DRM was evaluated by TPO analysis (Figure 7). Both catalysts (Ni-TNT500 and Ni-TNR) present a small weight increase between 300-500 °C, corresponding to 0.4 and 1.1% of Ni-TNT500 and Ni-TNR, respectively. This difference can correspond to the oxidation of nickel particles supported on the spent catalysts.[69] For the Ni-TNT500 is observed very small loss weight (ca. 3%) after the Ni oxidation, and a small weight loss (ca. 7%) is observed for Ni-TNR due to the oxidation of carbon deposited on the catalyst. The small weight loss observed in the catalysts after the reaction was probably due to oxidation of the carbon filaments, as shown in the TEM images.

At lower temperatures (300-500 °C), mass loss is related to the oxidation of C_α, while at temperatures between 600-700 °C, the oxidation of C_β occurs, with this carbon being responsible for catalytic deactivation processes.[68] As observed, neither of the catalysts promotes the formation of C_β.

The carbon production by Ni-TNR can be related to the higher CH_4 conversions during the reaction. By differential thermal analysis (DTA, Figure 7b) it is observed, for both catalysts, in lower temperatures (< 400 °C), the oxidation of a small amount of the amorphous carbon.[70,71] Considering the low weight variation in this range, the amount of amorphous carbon was small and similar for both samples. At 580 °C, DTA exhibits a peak related to the filamentous carbon oxidation.[56] The type of carbon formed can influence the stability of the catalysts. So, even if the Ni-TNR catalyst produced more carbon than Ni-TNT500 it can be stable if it produces structured

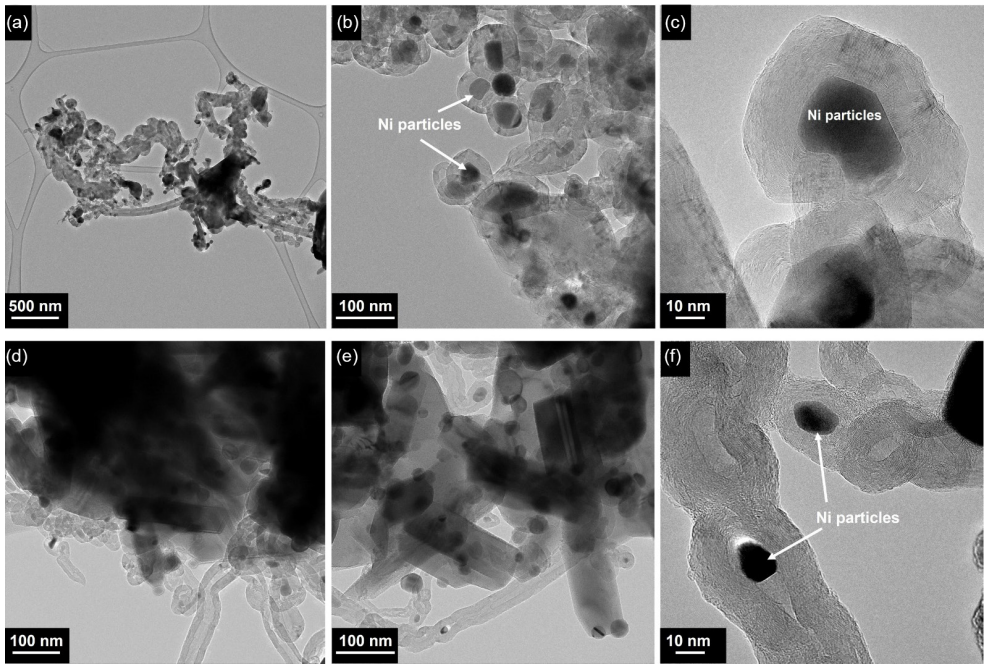

Figure 6. TEM images of spent catalyst: (a,b and c) Ni-TNT500 and (d,e and f) Ni-TNR.

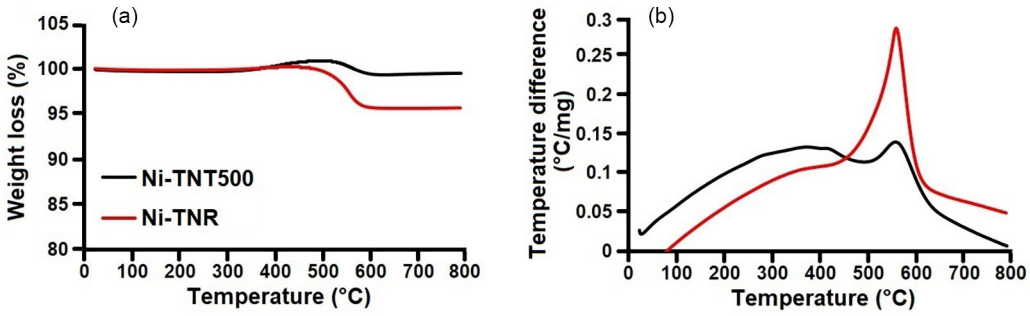

Figure 7. TPO analysis of spent catalysts (a) TG curves and (b) DTA curves.

carbon.[66] In addition, the carbon oxidation temperature close to 600 °C for Ni-containing catalysts used in the DRM reaction has been related to the oxidation of carbon filaments, i.e., structured carbon.[64]

Conclusions

This study presented the synthesis of titanate nanotubes calcined at 500 °C and titanate nanorods modified with Ni and their catalytic activity in the dry reforming of methane. Both supports (TNT500 and TNR) presented external diameter superior that found for pristine TNTs in a previous study. The morphology of TNT500 is similar to TNT, corresponding to nanotubes, while the calcination temperature of 700 °C leads to morphology change generating rod morphology. The structure of TNT500 is also similar to pristine TNT, but for TNR it was observed the presence of anatase and rutile phases of titanium and in both nanostructures. Regarding the deposition of Ni, a homogeneous distribution is observed in both catalytic systems, as evidenced by TEM and EDS analyses. CO_2 conversions from 7 to 60% and CH_4 conversions from 5 to 48% were obtained with Ni-TNT500 in the DRM reaction. When the Ni-TNR was used, CO_2 conversion ranged from 7 to 85%, while CH_4 conversion ranged from 7 to 70%. Additionally, carbon deposition was evaluated, and the analysis of spent catalysts revealed a low carbon deposition. These results outperformed the previous study conducted by the group, indicating that calcination not only influences the morphology or structure of titanates, but also promotes an increase in catalytic activity for the DRM reaction.

Acknowledgments

This study was financed in part by the Coordenação de Aperfeiçoamento de Pessoal de Nível Superior - Brasil (CAPES) - Finance Code 001. Wesley F. Monteiro and Michele O. Vieira thank the CNPq (PDJ process numbers

157931/2018-8 and 157767/2018-3, respectively). The authors would like to thank the National Council for Scientific and Technological Development (CNPq) and the Pontifical Catholic University of Rio Grande do Sul (PUCRS) and the Federal University of Rio Grande do Sul (UFRGS) for technical support, and the Central Laboratory of Microscopy and Microanalysis (LabCEMM/PUCRS) for the morphological analyses.

Author Contributions

Wesley F. Monteiro was responsible for conceptualization, data curation, formal analysis, investigation, writing original draft, review and editing; Vinícius D. da Silva for data curation, formal analysis, investigation, writing-review and editing; Michele O. Vieira for data curation, formal analysis, investigation, writing-review and editing; Camila O. Calgaro for data curation, formal analysis, investigation, writing-review and editing; Oscar W. Perez-Lopez for investigation, writing-review and editing; Marcus Seferin for investigation, resources, writing-review and editing; Rosane A. Ligabue for conceptualization, funding acquisition, investigation, project administration, resources, writing-review and editing.

References

1. Modak, A.; Jana, S.; *Microporous Mesoporous Mater.* **2019**, *276*, 107. [Crossref]
2. Tong, S.; Ebi, K.; *Environ. Res.* **2019**, *174*, 9. [Crossref]
3. Tsigaris, P.; Wood, J.; *Ecol. Econ.* **2019**, *162*, 74. [Crossref]
4. Skytt, T.; Nielsen, S. N.; Jonsson, B. G.; *Ecol. Indic.* **2020**, *110*, 105831. [Crossref]
5. United Nations, *Paris Agreement*, https://unfccc.int/sites/default/files/english_paris_agreement.pdf, accessed in April 2024.
6. Vieira, M. O.; Monteiro, W. F.; Ligabue, R.; Seferin, M.; Chaban, V. V.; Andreeva, N. A.; do Nascimento, J. F.; Einloft, S.; *J. Mol. Liq.* **2017**, *241*, 64. [Crossref]
7. Jung, S.; Park, Y. K.; Kwon, E. E.; *J. CO2 Util.* **2019**, *32*, 128. [Crossref]
8. Vieira, M. O.; Monteiro, W. F.; Neto, B. S.; Ligabue, R.; Chaban, V. V.; Einloft, S.; *Catal. Lett.* **2018**, *148*, 108. [Crossref]
9. Zhao, Y.; Wu, M.; Guo, X.; Zhang, Y.; Ji, Z.; Wang, J.; Liu, J.; Liu, J.; Wang, Z.; Chi, Q.; Yuan, J.; *Sep. Purif. Technol.* **2019**, *210*, 343. [Crossref]
10. Shehu, H.; Gobina, E.; Orakwe, I.; *Int. J. Hydrogen Energy* **2019**, *44*, 9896. [Crossref]
11. Imbiriba, B. C. O.; Ramos, J. R. S.; de Sousa Silva, R.; Cattanio, J. H.; do Couto, L. L.; Mitschein, T. A.; *Waste Manage.* **2020**, *101*, 28. [Crossref]
12. National Oceanic and Atmospheric Administration (NOAA), https://gml.noaa.gov/ccgg/trends/gl_trend.html, accessed in April 2024.
13. Wang, C.; Sun, N.; Zhao, N.; Wei, W.; Sun, Y.; Sun, C.; Liu, H.; Snape, C. E.; *Fuel* **2015**, *143*, 527. [Crossref]
14. Elvidge, C. D.; Bazilian, M. D.; Zhizhin, M.; Ghosh, T.; Baugh, K.; Hsu, F. C.; *Energy Strateg. Rev.* **2018**, *20*, 156. [Crossref]
15. Song, C.; Liu, Q.; Ji, N.; Deng, S.; Zhao, J.; Li, Y.; Song, Y.; Li, H.; *Renewable Sustainable Energy Rev.* **2018**, *82*, 215. [Crossref]
16. Bui, M.; Adjiman, C. S.; Bardow, A.; Anthony, E. J.; Boston, A.; Brown, S.; Fennell, P. S.; Fuss, S.; Galindo, A.; Hackett, L. A.; Hallett, J. P.; Herzog, H. J.; Jackson, G.; Kemper, J.; Krevor, S.; Maitland, G. C.; Matuszewski, M.; Metcalfe, I. S.; Petit, C.; Puxty, G.; Reimer, J.; Reiner, D. M.; Rubin, E. S.; Scott, S. A.; Shah, N.; Smit, B.; Trusler, J. P. M.; Webley, P.; Wilcox, J.; Mac Dowell, N.; *Energy Environ. Sci.* **2018**, *11*, 1062. [Crossref]
17. Baena-Moreno, F. M.; Rodríguez-Galán, M.; Vega, F.; Alonso-Fariñas, B.; Vilches Arenas, L. F.; Navarrete, B.; *Energy Sources, Part A* **2019**, *41*, 1403. [Crossref]
18. Gutiérrez-Guerra, N.; González, J. A.; Serrano-Ruiz, J. C.; López-Fernández, E.; Valverde, J. L.; de Lucas-Consuegra, A.; *J. Energy Chem.* **2019**, *31*, 46. [Crossref]
19. Vieira, M. O.; Monteiro, W. F.; Neto, B. S.; Chaban, V. V.; Ligabue, R.; Einloft, S.; *React. Kinet., Mech. Catal.* **2019**, *126*, 987. [Crossref]
20. Angeli, S. D.; Monteleone, G.; Giaconia, A.; Lemonidou, A. A.; *Int. J. Hydrogen Energy* **2014**, *39*, 1979. [Crossref]
21. Enger, B. C.; Lødeng, R.; Holmen, A.; *Appl. Catal., A* **2008**, *346*, 1. [Crossref]
22. Chein, R. Y.; Hsu, W.-H.; *Energy* **2019**, *180*, 535. [Crossref]
23. Fan, J.; Zhu, L.; Jiang, P.; Li, L.; Liu, H.; *J. Clean. Prod.* **2016**, *131*, 247. [Crossref]
24. Li, H.; He, Y.; Shen, D.; Cheng, S.; Wang, J.; Liu, H.; Xing, C.; Shan, S.; Lu, C.; Yang, R.; *Int. J. Hydrogen Energy* **2017**, *42*, 10844. [Crossref]
25. Ma, Q.; Han, Y.; Wei, Q.; Makpal, S.; Gao, X.; Zhang, J.; Zhao, T.; *J. CO2 Util.* **2020**, *35*, 288. [Crossref]
26. Hambali, H. U.; Jail, A. A.; Abdulrasheed, A. A.; Siang, T. J.; Vo, D.-V. N.; *J. Energy Inst.* **2020**, *93*, 1535. [Crossref]
27. Gavrilova, N. N.; Sapunov, V. N.; Skudin, V. V.; *Chem. Eng. J.* **2019**, *374*, 983. [Crossref]
28. Abbas, H. F.; Wan Daud, W. M. A.; *Int. J. Hydrogen Energy* **2010**, *35*, 1160. [Crossref]
29. Zhu, J.; Peng, X.; Yao, L.; Tong, D.; Hu, C.; *Catal. Sci. Technol.* **2012**, *2*, 529. [Crossref]
30. Tian, X.; Zeng, Y.; Xiao, T.; Yang, C.; Wang, Y.; Zhang, S.; *Microporous Mesoporous Mater.* **2011**, *143*, 357. [Crossref]
31. Asencios, Y. J. O.; Bellido, J. D. A.; Assaf, E. M.; *Appl. Catal., A* **2011**, *397*, 138. [Crossref]
32. Choque, V.; de la Piscina, P. R.; Molyneux, D.; Homs, N.; *Catal. Today* **2010**, *149*, 248. [Crossref]
33. Li, X.; Hu, Q.; Yang, Y.; Wang, Y.; He, F.; *Appl. Catal., A* **2012**, *413-414*, 163. [Crossref]

34. Asencios, Y. J. O.; Assaf, E. M.; *Fuel Process. Technol.* **2013**, *106*, 247. [Crossref]
35. Zhang, Q.; Tang, T.; Wang, J.; Sun, M.; Wang, H.; Sun, H.; Ning, P.; *Catal. Commun.* **2019**, *131*, 105782. [Crossref]
36. Pinto, D.; Hu, L.; Urakawa, A.; *Chem. Eng. J.* **2023**, *474*, 145641. [Crossref]
37. Guerrero-Caballero, J.; Kane, T.; Haidar, N.; Jalowiecki-Duhamel, L.; Löfberg, A.; *Catal. Today* **2019**, *333*, 251. [Crossref]
38. Chein, R. Y.; Fung, W. Y.; *Int. J. Hydrogen Energy* **2019**, *44*, 14303. [Crossref]
39. Mourhly, A.; Kacimi, M.; Halim, M.; Arsalane, S.; *Int. J. Hydrogen Energy* **2020**, *45*, 11449. [Crossref]
40. Da Costa, K. S.; Gálvez, M. E.; Motak, M.; Grzybek, T.; Rønning, M.; Da Costa, P.; *Catal. Commun.* **2018**, *117*, 26. [Crossref]
41. Kim, W. Y.; Jang, J. S.; Ra, E. C.; Kim, K. Y.; Kim, E. H.; Lee, J. S.; *Appl. Catal., A* **2019**, *575*, 198. [Crossref]
42. Oton, L. F.; Coelho, D. C.; Oliveira, A. C.; de Araujo, J. C. S.; Lang, R.; Rodríguez-Castellón, E.; Rodríguez-Aguado, E.; Lucredio, A. F.; Assaf, E. M.; Reyna-Alvarado, J.; López-Galán, O. A.; Ramos, M.; *Mol. Catal.* **2020**, *480*, 110641. [Crossref]
43. Chen, L.-W.; Ng, K. H.; *Process Saf. Environ. Prot.* **2024**, *183*, 244. [Crossref]
44. Grabchenko, M.; Pantaleo, G.; Puleo, F.; Kharlamova, T. S.; Zaikovskii, V. I.; *Catal. Today*. **2021**, *382*, 71. [Crossref]
45. Souza, H. T. S.; Oliveira, S. A. A.; Souza, J. S.; *J. Photochem. Photobiol., A* **2020**, *390*, 112264. [Crossref]
46. Vranješ, M.; Jakovljević, J. K.; Milošević, M.; Ćirić-Marjanović, G.; Stoiljković, M.; Konstantinović, Z.; Pavlović, V.; Milivojević, D.; Šaponjić, Z.; *Solid State Sci.* **2019**, *94*, 155. [Crossref]
47. Fernández-Werner, L.; Pignanelli, F.; Montenegro, B.; Romero, M.; Pardo, H.; Faccio, R.; Mombrú, Á. W.; *J. Energy Storage* **2017**, *12*, 66. [Crossref]
48. Esteves, M.; Fernández-Werner, L.; Pignanelli, F.; Romero, M.; Chialanza, M. R.; Faccio, R.; Mombrú, Á. W.; *Ceram. Int.* **2020**, *46*, 2877. [Crossref]
49. Thu, D. T.; Hien, H. T.; Thu, D. T. A.; Ngan, P. Q.; Thai, G. H.; van Tuan, C.; Trung, T.; Giang, H. T.; *Sensors Actuators, B* **2017**, *244*, 941. [Crossref]
50. Gusmão, S. B. S.; Ghosh, A.; Marques, T. M. F.; Ferreira, O. P.; Lobo, A. O.; Osajima, J. A. O.; Luz-Lima, C.; Sousa, R. R. M.; Matos, J. M. E.; Viana, B. C.; *J. Nanomater.* **2019**, *2019*, ID 4825432. [Crossref]
51. Lima, G. R.; Monteiro, W. F.; Toledo, B. O.; Ligabue, R. A.; Santana, R. M. C.; *Macromol. Symp.* **2019**, *383*, 1800008. [Crossref]
52. Sluban, M.; Cojocaru, B.; Parvulescu, V. I.; Iskra, J.; Korosec, R. C.; Umek, P.; *J. Catal.* **2017**, *346*, 161. [Crossref]
53. Martínez-Klimov, M. E.; Hernández-Hipólito, P.; Martínez-García, M.; Klimova, T. E.; *Catal. Today* **2018**, *305*, 58. [Crossref]
54. Zaki, A. H.; Naeim, A. A.; EL-Dek, S. I.; *Environ. Sci. Pollut. Res.* **2019**, 36388. [Crossref]
55. Coelho, D. C.; Oliveira, A. C.; Filho, J. M.; Oliveira, A. C.; Lucredio, A. F.; Assaf, E. M.; Rodriguez-Castellón, E.; *Chem. Eng. J.* **2016**, *290*, 438. [Crossref]
56. Monteiro, W. F.; Vieira, M. O.; Calgaro, C. O.; Perez-Lopez, O. W.; Ligabue, R. A.; *Fuel* **2019**, *253*, 713. [Crossref]
57. Scheid, C. M.; Monteiro, W. F.; Vieira, M. O.; Alban, L.; Luza, L.; Eberhardt, D.; Gonçalves, R. V.; Feil, A. F.; Lima, J. E. A.; Ligabue, R. A.; *Chem. Eng. Res. Des*. **2023**, *197*, 392. [Crossref]
58. Wittich, K.; Kramer, M.; Bottke, N.; Schunk, S. A.; *ChemcatChem*. **2020**, *12*, 2130. [Crossref]
59. Viana, B. C.; Ferreira, O. P.; Filho, A. G. S.; Hidalgo, A. A.; Filho, J. M.; Alves, O. L.; *Vib. Spectrosc.* **2011**, *55*, 183. [Crossref]
60. Gomes, I. S.; de Carvalho, D. C.; Oliveira, A. C.; Rodríguez-Castellón, E.; Tehuacanero-Cuapa, S.; Freire, P. T. C.; Filho, J. M.; Saraiva, G. D.; de Sousa, F. F.; Lang, R.; *Chem. Eng. J.* **2018**, *334*, 1927. [Crossref]
61. Lima, G. R.; Monteiro, W. F.; Scheid, C. M.; Ligabue, R. A.; Santana, R. M. C.; *Catal. Lett.* **2019**, *149*, 1415. [Crossref]
62. Jin, S.; Wang, Z.; Tao, G.; Zhang, S.; Liu, W.; Fu, W.; Zhang, B.; Sun, H.; Wang, Y.; Yang, W.; *J. Catal.* **2017**, *353*, 305. [Crossref]
63. Benrabaa, R.; Barama, A.; Boukhlouf, H.; Guerrero-Caballero, J.; Rubbens, A.; Bordes-Richard, E.; Löfberg, A.; Vannier, R. N.; *Int. J. Hydrogen Energy* **2017**, *42*, 12989. [Crossref]
64. Liu, H.; Wierzbicki, D.; Debek, R.; Motak, M.; Grzybek, T.; Da Costa, P.; Gálvez, M. E.; *Fuel* **2016**, *182*, 8. [Crossref]
65. Nikoo, M. K.; Amin, N. A. S.; *Fuel Process. Technol.* **2011**, *92*, 678. [Crossref]
66. Calgaro, C. O.; Perez-Lopez, O. W.; *Int. J. Hydrogen Energy* **2019**, *44*, 17750. [Crossref]
67. Calgaro, C. O.; Perez-Lopez, O. W.; *Int. J. Hydrogen Energy* **2017**, *42*, 29756. [Crossref]
68. Al-Fatesh, A. S.; Fakeeha, A. H.; Khan, W. U.; Ibrahim, A. A.; He, S.; Seshan, K.; *Int. J. Hydrogen Energy* **2016**, *41*, 22932. [Crossref]
69. Li, K.; Pei, C.; Li, X.; Chen, S.; Zhang, X.; Liu, R.; Gong, J.; *Appl. Catal., B* **2020**, *264*, 118448. [Crossref]
70. Wei, T.; Jia, L.; Luo, J. L.; Chi, B.; Pu, J.; Li, J.; *Appl. Surf. Sci.* **2020**, *506*, 144699. [Crossref]
71. Kim, H.; Robertson, A. W.; Kwon, G. H.; Jang-Won, O.; Warner, J. H.; Kim, J. M.; *ACS Appl. Energy Mater.* **2019**, *2*, 8649. [Crossref]

Submitted: November 1, 2023
Published online: April 26, 2024